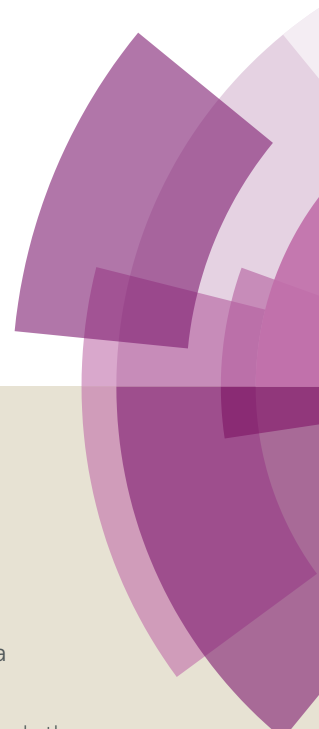


Dalton Transactions

Accepted Manuscript



This article can be cited before page numbers have been issued, to do this please use: A. Liberato, A. Aguinaco, M. P. Clares, E. Delgado-Pinar, S. Blasco, J. Pitarch-Jarque, M. G. Basallote, E. García-España and B. Verdejo, *Dalton Trans.*, 2017, DOI: 10.1039/C7DT00680B.



This is an Accepted Manuscript, which has been through the Royal Society of Chemistry peer review process and has been accepted for publication.

Accepted Manuscripts are published online shortly after acceptance, before technical editing, formatting and proof reading. Using this free service, authors can make their results available to the community, in citable form, before we publish the edited article. We will replace this Accepted Manuscript with the edited and formatted Advance Article as soon as it is available.

You can find more information about Accepted Manuscripts in the [author guidelines](#).

Please note that technical editing may introduce minor changes to the text and/or graphics, which may alter content. The journal's standard [Terms & Conditions](#) and the ethical guidelines, outlined in our [author and reviewer resource centre](#), still apply. In no event shall the Royal Society of Chemistry be held responsible for any errors or omissions in this Accepted Manuscript or any consequences arising from the use of any information it contains.



Journal Name

ARTICLE

Pb²⁺ Complexes of Small-Cavity Azamacrocyclic Ligands. Thermodynamic and Kinetic Studies.

A. Liberato,^a A. Aguinaco,^a M. P. Clares,^b E. Delgado-Pinar,^b J. Pitarch-Jarque,^b S. Blasco,^b M. G. Basallote,^{*a} E. García-España^{*b} and B. Verdejo^{*b}

Received 00th January 20xx,
Accepted 00th January 20xx

DOI: 10.1039/x0xx00000x

www.rsc.org/

The synthesis, acid–base behavior and Pb²⁺ coordination chemistry of the new aza-scorpianid like ligand 5-[2-(N-2-fluorenyl)ethylamino]-2,5,8-triaza[9]-2,6-pyridinophane (**L1**) have been studied by potentiometry, NMR and spectrofluorimetric titrations, and the results are compared with those obtained for the related compounds **L2**, lacking of the fluorenyl group, and **L3**, the macrocycle lacking of pendant arm. The crystal structures obtained for the complexes [Pb**L1**][Pb**L1**Cl](NO₃)Cl₂·4H₂O (**1**) and [Pb**L3**](ClO₄)₂ (**2**) reveal that the metal ion is located over the plane defined by the nitrogen atoms of the macrocyclic core due to its inability to accommodate the large Pb²⁺ ion in the macrocyclic cavity. For **L1**, the secondary amino group of the pendant arm is implicated in the coordination of the metal ion, although the stereoactive lone pair of Pb²⁺ prevents the closed conformation associated to the coordination of metal ions in aza-scorpianid derivatives. The kinetics of the acid-promoted dissociation of the ligand from the Pb²⁺ complexes with the three ligands has been studied using stopped-flow with simultaneous absorbance and fluorescence detection. The results indicate that in spite of their similarity, the dissociation of the metal ion occurs with very different rates in the three complexes. During the course of the kinetic studies evidence was obtained for the occurrence of a photochemical process that leads to ligand degradation with the unexpected elimination of one CH₂CH₂ fragment from the macrocyclic core.

Introduction

Lead is considered as an environmental pollutant with severe toxic effects for human healthcare.¹ In fact, different enzymes involved in the heme biosynthesis are inhibited by Pb²⁺ like *porphobilinogen synthase* or *ferrochelatase*, which catalyzes the introduction of iron into the heme precursor, causing haematological effects.^{2,3} Current treatments of lead intoxication involve various chelating agents, but these are usually nonspecific and relatively toxic.⁴ In this sense, studies on the stability and chemical properties of Pb²⁺ complexes have aroused great interest, an important issue frequently discussed being the stereochemical activity of the lone-electron pair and the coordination sphere distortions associated to it.⁵⁻⁷

During the last years, we have studied the Cu, Zn or Mn coordination chemistry of aza-scorpianid ligands and their properties as antioxidant and/or antitumoral agents.^{8,9} In the

ML complexes of these ligands, the metal ion is strongly coordinated by the amino groups present in the macrocyclic cavity and the pendant arm, acquiring the classical “closed” conformation of the scorpianid ligands.^{9,10} Although an interesting study on a lead-π interaction achieved during the templating formation of a Schiff base oxa-aza-scorpianid ligand has been recently reported,¹¹ the formation of Pb²⁺ complexes by these saturated aza-macrocyclic scorpianid ligands had not been explored yet. Herein, we report the preparation of a new receptor functionalised with a 2-fluorenyl group (**L1** in Chart 1) aimed to facilitate fluorescence detection. Although we had previously reported on related ligands with naphthyl or anthryl groups,^{9,10} the use of a fluorenyl group shows advantages due to its photophysical properties and because of solubility issues. Working with a naphthyl instead of the fluorenyl leads to a much less intense fluorescence and therefore to a poorer sensing behaviour. On the other hand, the use of both naphthalene and anthracene gives rise to solubility issues with the lead complexes. In this paper, we present the protonation behaviour of the new ligands, the formation of Pb²⁺ complexes both in solution and in the solid state. For comparison, studies have been also carried out with the parent ligands **L2** and **L3**.^{10,12}

For a better understanding of the solution properties of these complexes, the equilibrium studies are complemented with kinetic studies on the acid-promoted dissociation of the Pb²⁺ complexes, which has previously provided relevant information on the occurrence of structural reorganizations of

^a Departamento de Ciencia de los Materiales e Ingeniería Metalúrgica y Química Inorgánica, Facultad de Ciencias, Universidad de Cádiz, Avenida República Saharaui s/n, 11510, Puerto Real (Cádiz, Spain), E-mail: manuel.basallote@uca.es

^b Instituto de Ciencia Molecular, Departamento de Química Inorgánica, Universidad de Valencia, Edificio de Institutos de Paterna, C/Catedrático José Beltrán 2, 46980, Paterna (Valencia, Spain) E-mail: enrique.garcia-es@uv.es, begona.verdejo@uv.es.

† Electronic Supplementary Information (ESI) available: Distribution diagrams, fluorescence and electronic spectra, crystallographic data (CCDC-1528996, CCDC-1529381) and selected distances and angles are included. See DOI: 10.1039/x0xx00000x

ARTICLE

Journal Name

Cu^{2+} scorpionand complexes involving the donor atoms in the tail.^{10,13,14} In spite that many kinetic studies had been conducted for other metal ions, the number of kinetic studies dealing with Pb^{2+} complexes is rather limited.¹⁵ In addition, the fluorescence properties of the ligand can be used to monitor the kinetics using simultaneous absorbance and fluorescence detection, an approach that proved to be especially useful for detecting structural reorganizations in a recent study dealing with an indazole-containing ligand.¹⁴ In the present case, those studies have allowed for the observation of an unexpected photochemical decomposition of the macrocycle.

Additional studies were carried out using the fluorescence emission spectra and the NMR spectra at different pH values, as they can give indications of the protonation sequence followed by polyamine ligands. In a similar way to other aza-scorpionand ligands previously reported,^{9,10} the fluorescence emission spectra of **L1** recorded at variable pH show a quenching effect when passing from $[\text{H}_3\text{L}]^{3+}$ to $[\text{H}_2\text{L}]^{2+}$. This effect can be attributed to a photoinduced electron transfer (PET) process,¹⁷ denoting that deprotonation of the secondary amino group closest to the fluorene fragment is occurring at this stage (Fig. 1).

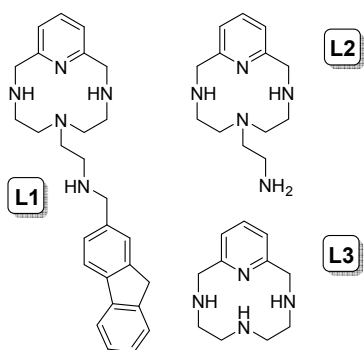


Chart 1. Drawing of the ligands.

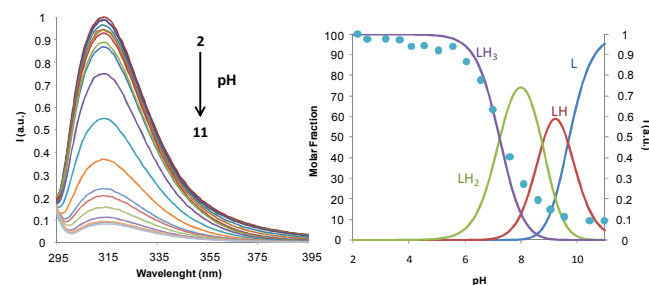


Fig. 1 (left) Fluorescence emission spectra of **L1** recorded at 298.1 K as function of pH. (right) Steady-state fluorescence emission titration curve of **L1** ($\lambda_{\text{exc}} = 285$ nm) measured at 298.1 ± 0.1 K with $[\text{L1}] = 1.0 \times 10^{-5}$ M (blue ●) and mole fraction distribution curves for the different protonated forms (solid lines).

Results and discussion

Equilibrium studies on ligand protonation and Pb^{2+} coordination. As a necessary previous step for the determination of the stability constants of Pb^{2+} complexes we have firstly studied the acid-base behavior of the free ligands.¹⁶ The stepwise protonation constants of **L1** were determined from potentiometric studies in 0.15 M NaNO_3 at 298.1 K, and the results are collected in Table 1 along with those previously reported for **L2** and **L3**.^{10,12} The distribution diagram of the different protonated species formed by **L1** is collected in Figs. 1 right and S1. **L1** presents in the pH range of study (2.5–11.0) three relatively high stepwise constants separated by *ca.* 1.3 logarithmic units that correspond to the protonation of the secondary amino groups of the molecule. Interestingly, all the three constants are lower than the corresponding ones of **L2** and **L3**, probably due to the hydrophobic environment generated by the fluorene moiety.

Table 1 Logarithms of the stepwise protonation constants for **L1** determined at 298.1 K in 0.15 M NaNO_3 ; the corresponding values for **L2** and **L3** are also included for comparison.^{10,12}

Reaction ^a	L1	L2 ^c	L3 ^d
$\text{H} + \text{L} \rightleftharpoons \text{HL}$	9.68(1) ^b	10.20(6)	10.33(4)
$\text{H} + \text{HL} \rightleftharpoons \text{H}_2\text{L}$	8.75(1)	9.18(3)	7.83(5)
$\text{H} + \text{H}_2\text{L} \rightleftharpoons \text{H}_3\text{L}$	7.32(1)	7.84(4)	1.27

a) Charges omitted. b) Values in parenthesis are standard deviations in the last significant figure. c) Determined in 0.15 M NaClO_4 . d) Determined in 0.1 M KNO_3 .

The upfield shift observed for the ^1H signals associated to the fluorene moiety on going from pH 3 to pH 8 (Fig. 2) adds further support to this proposal. However, as reported for analogous aza-scorpionand ligands, an upfield shift of the ^1H signals of both aromatic rings, in this case pyridine and fluorene, can be also associated with a molecular rearrangement in which the pendant arm approaches the macrocyclic core giving a π -stacking interaction as a result of a change in the protonation state of the ligand.¹⁰

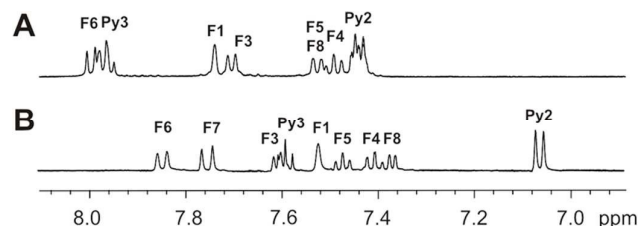


Fig. 2 ^1H NMR spectra of the aromatic region of **L1** recorded in D_2O at pH: (A) 3.23 and (B) 8.58.

The equilibrium constants for the Pb^{2+} complexes were also determined from pH-metric titrations carried out at 298.1 K in 0.15 M NaNO_3 , and the analysis of the data lead to the equilibrium model and stability constants shown in Table 2. Only mononuclear species, $[\text{Pb}(\text{H}_x\text{L})]^{(2+x)+}$ with protonation degrees *x* varying from -1 to 1 for **L1** and **L2** and from 1 to 0 for **L3**, have been detected. Comparison of the stability constants of **L1** with those of the related ligands **L2** and **L3** suggest at least four as the number of nitrogen of the constant obtained for the Pb^{2+} . In addition, the lower value of the constant obtained for the

equilibrium $[\text{PbL1}]^{2+} + \text{H}^+ \rightleftharpoons [\text{PbHL1}]^{3+}$ ($\log K = 5.719(6)$) in comparison to $[\text{H}_2\text{L1}]^{2+} + \text{H}^+ \rightleftharpoons [\text{H}_3\text{L1}]^{3+}$ ($\log K = 7.32(1)$) (stepwise protonation constant of the free receptor at the stage at which both reactions display the same charges) suggests that the amino group of the pendant arm is also involved in the coordination to the metal, a suggestion further supported by the crystal structure of the Pb-L1 complex described below.

Table 2 Logarithms of the formation constants of Pb^{2+} complexes with L1-L3 determined at 298.1 K in 0.15 M NaNO_3 (L1) and 0.15 M NaClO_4 (L2 and L3).

Reaction	L1	L2	L3
$\text{M} + \text{L} \rightleftharpoons \text{ML}^{\text{a}}$	14.69(1) ^b	15.22(3)	15.71(3)
$\text{ML} + \text{H} \rightleftharpoons \text{MLH}$	5.719(6)	6.69(3)	3.42(8)
$\text{ML} + \text{H}_2\text{O} \rightleftharpoons \text{ML}(\text{OH}) + \text{H}$	-10.77(2)	-11.37(5)	-

a) Charges omitted. b) Values in parenthesis are standard deviations in the last significant figure.

Fig. 3 shows the steady-state fluorescence emission titration curves of the Pb^{2+} -L1 system (1:1 molar ratio). The major difference with the curve in the absence of Pb^{2+} is the observation of a strong quenching effect that starts with the formation of the protonated complex species $[\text{PbHL1}]^{3+}$. The quenching becomes total with the formation of the non-protonated $[\text{PbL1}]^{2+}$ complex. This finding is in agreement with expectations for a complete cancellation of ligand emission upon coordination with a heavy metal ion as Pb^{2+} .¹⁸ This perturbation of the fluorescence will permit the detection of Pb^{2+} with a lower detection limit of 3.0 ± 0.2 ppb which lies clearly below the 15 ppb maximum amount recommended by the USA Environmental Protection Agency (EPA) for drinking water (See Fig S2).¹⁹

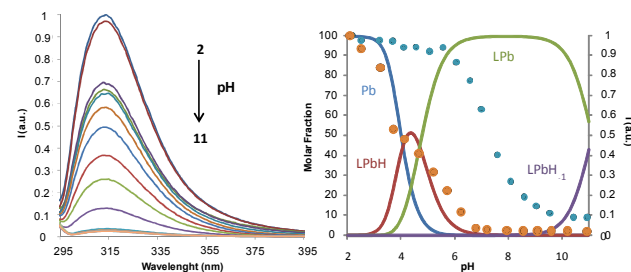


Fig. 3 (left) Fluorescence emission spectra of Pb^{2+} -L1 recorded at 298.1 K as a function of pH. (right) Steady-state fluorescence emission titration curves for the system Pb^{2+} -L1 ($\lambda_{\text{exc}} = 285$ nm) in a 1:1 molar ratio M:L ($[\text{L1}] = [\text{Pb}^{2+}] = 10^{-5}$ M. Emission followed at 312 nm (free ligand ● blue, metal complexes ● orange) and mole fraction distribution curves for the Pb^{2+} complexes (solid lines).

Crystallographic studies. The involvement of the secondary amino group of the pendant arm in the coordination to the metal ion is supported by the crystal structure of the complex $[\text{PbL1}][\text{PbL1Cl}](\text{NO}_3)_2 \cdot 4\text{H}_2\text{O}$ (**1**) (Fig. 4).

The crystal structure contains two cationic species $[\text{PbL1Cl}]^+$ (Fig. 4a), $([\text{PbL1}](\text{NO}_3)(\text{H}_2\text{O}))^+$ (Fig. 4b), two chloride anions that form hydrogen bonds with the amines N4a and N4b, and three water molecules. In both cationic complexes, the metal ion is coordinated to the four nitrogen atoms of the macrocyclic

cavity and to the secondary amino group of the pendant arm. However, while in $[\text{PbL1Cl}]^+$ there is a coordinated chloride anion with a bond distance of 2.912 Å (average Pb-Cl bond distances in Pb^{2+} complexes is 2.88 Å), in $([\text{PbL1}](\text{NO}_3)(\text{H}_2\text{O}))^+$ there are a water molecule and a NO_3^- (Pb-O distances 3.03 and 3.09 Å, respectively) which present just a very weak interaction with the metal ion (average Pb-O bond distance in Pb^{2+} complexes is 2.53 Å).⁵ The Pb^{2+} is placed in both units ca. 1.5 Å above the mean plane defined by the nitrogen atoms of the macrocyclic core. Both coordination spheres can be classified as hemidirected displaying a gap (Fig. 4), which is assumed to be occupied by the stereochemically active lone pair.^{5,6,7} The distances opposite to the lone pair are the shortest ones. The stereoactive effect of the lone pair seems to prevent the complex from adopting the closed conformation which is typically found in other metal complexes of this kind of aza-scorpand like ligands.^{8,9,10,14}

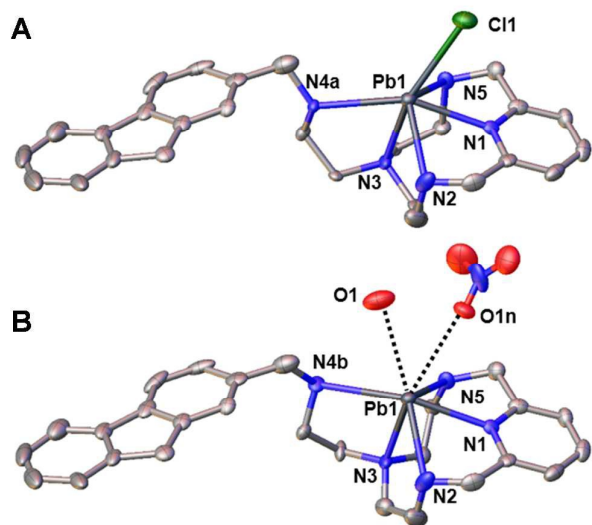
Table 3 Selected Bond Distances (Å) and Angles (deg) of complex **1**.

Bond Distances (Å)			Bond Angles (deg)			
Pb1	N1	2.526(9)	N1	Pb1	Cl1	76.0(4)
Pb1	N2	2.639(10)	N1	Pb1	N2	64.1(3)
Pb1	N5	2.510(9)	N1	Pb1	N3	86.9(3)
Pb1	N3	2.586(10)	N1	Pb1	N4B	154.2(4)
Pb1	N4A	2.90(2)	N1	Pb1	N4A	150.2(4)
Pb1	N4B	2.733(17)	N2	Pb1	Cl1	119.2(4)
Pb1	Cl1	2.912(16)	N2	Pb1	N4B	98.9(5)
Pb1	O1N	3.09(5)	N2	Pb1	N4A	116.2(5)
Pb1	O1	3.03(2)	N5	Pb1	Cl1	81.8(4)
			N5	Pb1	N1	65.0(3)
			N5	Pb1	N2	116.1(3)
			N5	Pb1	N3	71.6(3)
			N5	Pb1	N4B	111.1(5)
			N5	Pb1	N4A	91.8(5)
			N3	Pb1	Cl1	152.6(4)
			N3	Pb1	N2	69.6(4)
			N3	Pb1	N4B	68.3(4)
			N3	Pb1	N4A	67.3(4)
			N4B	Pb1	Cl1	129.7(5)

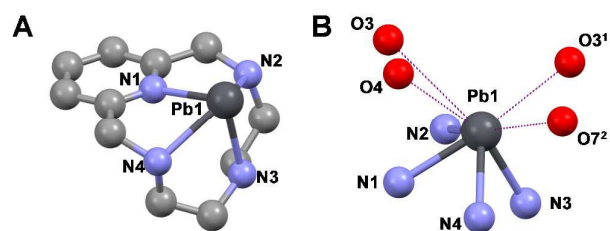
As occurs for L1, the X-ray crystal structure of $[\text{PbL3}](\text{ClO}_4)_2$, reveals that the metal ion is located ca. 1.5 Å over the plane defined by the four nitrogen atoms in the hemidirected coordination sphere (see Fig. 5). At the side of the stereoactive lone pair, there are four oxygen atoms (2.96-3.22 Å, see Table 4) coming from perchlorate counterions that have weak interaction with the metal ion (2.96-3.22 Å, see Table 4).

Table 4 Selected distances and angles for [PbL3](ClO₄)₂

Bond Distances (Å)		Bond Angles (deg)	
Pb-N1	2.400(8)	N1-Pb-N2	68.1(3)
Pb-N2	2.524(9)	N1-Pb-N4	65.9(3)
Pb-N3	2.42(1)	N1-Pb-N3	87.4(3)
Pb-N4	2.502(9)	N3-Pb-N4	53.1(3)
Pb-O4	3.11(2)	N3-Pb-N2	52.2(3)
Pb-O3	3.22(1)		
Pb-O3 ¹	2.96(1)		
Pb-O7 ²	3.11(1)		

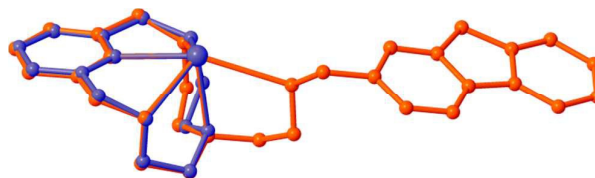
a) **1**: 1-x; 1-y; -z. b) **2**: 1-x; ½ + y; ½ -z.**Fig. 4** Ellipsoid representation of the cationic species: a) [(PbL1)(NO₃)(H₂O)]⁺ and b) [PbL1Cl]⁺. Thermal ellipsoids are shown at the 50% probability level. Hydrogen atoms have been omitted for clarity

As commented above, different structural effects have been proposed for previously reported Pb²⁺ complexes with macrocyclic ligands in which the presence of the stereoactive lone pair can be inferred.²⁰ These structural effects include the presence of an apparent gap in the coordination geometry and Pb²⁺-N bond distances opposite to the position of the lone pair shorter than those observed for “non-active” complexes (2.6–2.9 Å).⁵

**Fig. 5** (A) Ball and stick representation of the [PbL3]²⁺ cation. Hydrogens are not shown. (B) Coordination site of Pb²⁺ in [PbL3](ClO₄)₂ showing the gap occupied by the lone pair.

Interestingly enough, both structures present a very high degree of similarity when they are overlapped. The conformation of the macrocyclic core and disposition of the

lead atom is the same, independently of the fact that in **1** the secondary amino group of the pendant arm is also coordinated (See Fig. 6).

**Fig. 6** Overlay representation of crystals [PbL1]²⁺ (orange) and [PbL3]²⁺ (blue) in order to highlight the similarities in the geometry of the ligand. Only the metal complexes are shown

Kinetic studies on the acid-promoted dissociation of the Pb²⁺-L complexes. According to the potentiometric equilibrium studies, addition of an excess of acid to a solution containing any of the complexes commented above must result in complex decomposition with release of Pb²⁺ and protonated ligand. Although there are no many kinetic studies for Pb²⁺ complexes,¹⁵ the process has been comprehensively studied for other metal ions, especially for Cu²⁺. For the latter ion, this kind of kinetic studies has provided information not only on the dissociation of the metal ion but also on the existence of structural reorganizations between the different species that can be formed in solution.^{10,21,22} For this reason, kinetic studies on the acid-promoted decomposition of the Pb²⁺ complexes were undertaken. Because of the lack of absorption in the visible of the lead complexes, the kinetic experiments were carried out using simultaneous absorbance and fluorescence detection, a strategy that has recently revealed to be very useful for detecting indazole tautomerization during decomposition of a Cu²⁺ complex with a scorpion-like macrocycle.¹⁴

For each Pb²⁺ complex, the detection wavelength was selected according to both the absorption and excitation fluorescence spectra in such a way that the fluorescence signal was maximized while still showing absorbance changes. In this way the kinetics of decomposition of the Pb²⁺ complexes with **L1**, **L2** and **L3** were studied with a stopped-flow instrument by measuring the absorbance decrease at 285, 265 and 275 nm, respectively, with simultaneous recording of the fluorescence changes caused by excitation at the same wavelengths. For all the three ligands the kinetic studies were carried out with solutions containing Pb²⁺ and L in 1:1 molar ratio and the pH adjusted to values at which the corresponding [PbL]²⁺ and [Pb(HL)]³⁺ reach the maximum concentration in the species distribution curves.

In the case of **L3**, solutions with the initial pH adjusted to 8.5 and 3.3 respectively, were used. At pH 8.5 solutions contain exclusively [PbL3]²⁺, whereas at pH 3.3 there is a mixture of [PbL3]²⁺ and [Pb(HL3)]³⁺ in addition to Pb²⁺ and protonated ligand, the latter species being inactive in the process of complex decomposition. In all cases, both the absorbance and fluorescence traces showed changes that could be fitted satisfactorily to a single exponential, but the fluorescence changes were always slower than the absorbance changes (Fig.

7), the differences being more important for experiments with a starting pH of 8.5. The observed rate constants change linearly with the acid concentration (Fig. 8) and fitting the data to eq. 1 leads to the values of the second order rate constant (k) in Table 5. The values derived from the absorbance changes are similar for both species, which suggests that protonation of $[\text{PbL3}]^{2+}$ to form $[\text{Pb}(\text{HL3})]^{3+}$ is fast. However, the fact that the differences between the values derived from fluorescence data are larger, and always smaller than the absorbance-derived values, suggests that some additional process is occurring in solution.

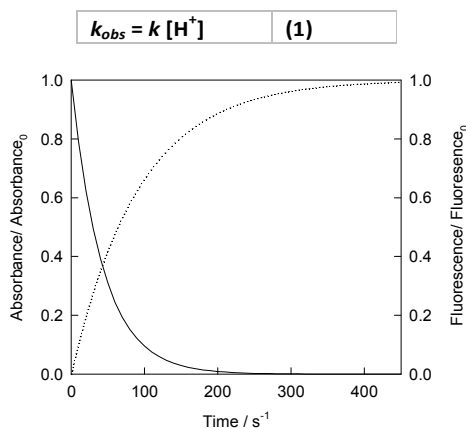


Fig. 7 Kinetic traces showing the absorbance (275 nm) (solid line) and fluorescence (excitation at 275 nm and detection at wavelengths larger than 295 nm) (dotted line) changes upon addition of an excess of acid (0.15 M) to a solution containing Pb^{2+} and **L3** ($[\text{Pb}]_0 = [\text{L3}]_0 = 5 \times 10^{-4}$ M) with the starting pH adjusted to 8.5. Both traces were recorded simultaneously on the same solution.

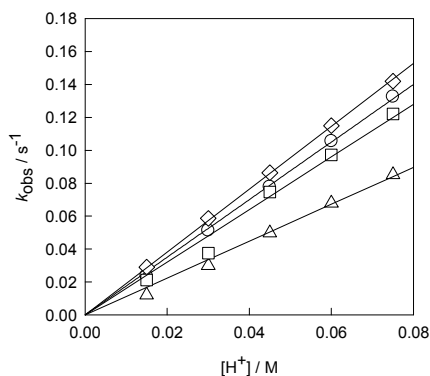


Fig. 8 Plots showing the dependence with the acid concentration of the observed rates constants for the decomposition of the Pb^{2+} -**L3** complexes: starting pH of 8.5 ($[\text{PbL3}]^{2+}$) with absorbance (circles) and fluorescence (triangles) detection, and starting pH of 3.3 (mixture of $[\text{Pb}(\text{HL3})]^{3+}$ and $[\text{PbL3}]^{2+}$) with absorbance (diamonds) and fluorescence (squares) detection.

Kinetic experiments were also carried out on the decomposition of the Pb^{2+} -**L2** complexes. In this case, the pH of the starting solutions was adjusted to 9 and 5, where solutions can be considered to contain exclusively the $[\text{PbL2}]^{2+}$ and $[\text{Pb}(\text{HL2})]^{3+}$ species, respectively. The results were quite similar to those observed for **L3**. The kinetic traces can be

always fitted to a single exponential and the values derived for the rate constants are lower from the fluorescence changes.

Table 5 Summary of second order rate constants (k) for the decomposition of the Pb^{2+} -L complexes with ligands **L2** and **L3**.

Ligand	Species	$k / \text{M}^{-1}\text{s}^{-1}$	
		Absorbance	Fluorescence
L3	$[\text{PbL3}]^{2+}$	1.75 ± 0.01	1.12 ± 0.03
	$[\text{Pb}(\text{HL3})]^{3+}$ ^a	1.91 ± 0.01	1.60 ± 0.05
L2	$[\text{PbL2}]^{2+}$	1.14 ± 0.02	0.92 ± 0.02
	$[\text{Pb}(\text{HL2})]^{3+}$	1.28 ± 0.01	1.06 ± 0.01

^a The starting solution also contains some amounts of $[\text{PbL3}]^{2+}$

The values derived for the second order rate constant are included in Table 5, and they also suggest that $[\text{PbL2}]^{2+}$ converts to $[\text{Pb}(\text{HL2})]^{3+}$ in a process that occurs within the mixing time of the stopped-flow instrument, although the smaller values of the fluorescence-derived rate constants again suggest the existence of an additional process.

For $[\text{PbL1}]^{2+}$, the decomposition process takes place within the mixing time of the stopped-flow instrument (*ca.* 1.7 ms) even at very low concentration of acid. The absence of spectral changes in the stopped-flow time scale was confirmed with independent experiments using a diode array detector. Nevertheless, for longer time significant variations in fluorescence were observed, which suggests changes in the ligand.

Regarding the decomposition rates of the Pb^{2+} complexes, it is remarkable that they are faster than those previously observed for the analogous Cu^{2+} complexes,¹⁰ which have a second order dependence on the acid concentration with k_{obs} values significantly smaller than those obtained in the present work. The faster decomposition of the Pb^{2+} complexes can be interpreted as resulting from the higher strain introduced in the complexed ligand by the larger size of Pb^{2+} with respect to Cu^{2+} .²³ On the other hand, the observation of faster decomposition of the Pb -**L1** complexes with respect to their Pb -**L3** analogous is surprising given the similarity of the crystal structures in Fig. 6. However, it has been shown previously that the kinetics of the acid-promoted dissociation of metal ions from polydentate amines is strongly dependent on the steric constraints imposed by coordination. The present results suggest that the small changes existing in the complexes with both ligands are enough to make dissociation to be faster enough in the **L1** complexes, making it to occur within the mixing time. Another possibility is that the structures of both complexes are not so similar in solution and that some reorganization of the metal-macrocycle core could accompany dissociation of the weakly bound anions.

Nevertheless, the most striking finding in the present kinetic studies is the observation of significantly slower decomposition when fluorescence is used for detection. These differences cannot be assigned to any change in the sample or experimental conditions as kinetic traces showing absorbance and fluorescence changes were always obtained simultaneously with the same solution. So, there must be some additional factor making slower the fluorescence

ARTICLE

Journal Name

changes. Careful inspection of curves as those in Fig. 7 show that whereas the absorbance changes are completed within the recording time, the fluorescence still keeps changing slightly. To obtain more information on this point, experiments using solutions of **L1-L3** without any added metal ion were also carried out. For the ligands both absorbance and fluorescence measurements showed slow changes that are not completed within the measuring time of the stopped-flow instrument (up to *c.a.* 2000 s). The changes are more important in the case of fluorescence, which keeps changing for very long recording times. These observations led us to think in the possibility of any photochemical process leading to ligand degradation, an assumption confirmed by additional photolysis experiments with NMR monitoring. Thus, to gain insight into the nature of the photolysed products, the ^1H NMR and DOSY spectra of a sample of **L3** photolysed for 20 hours with the same 150W Xe lamp used in the stopped-flow instrument were recorded. For comparison, Fig. 9 shows the spectrum of **L3** before photolysis. Due to the symmetry of the molecule two peaks appear in the aromatic region of the ^1H NMR spectrum corresponding to the protons (one for the equivalent PY2 and PY4, and another one for PY3) located in the pyridine ring. In the aliphatic region there are three signals associated to the protons labelled 1-3; the singlet at 4.45 ppm corresponding to the benzylic protons and the triplets at 2.7-3.1 ppm corresponding to the ethylenic protons.

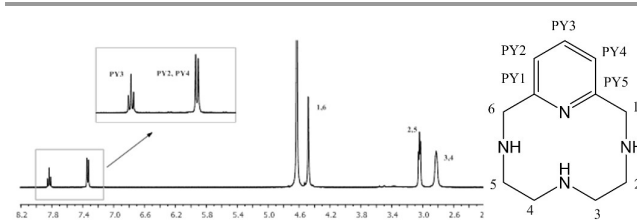


Fig. 9 ^1H NMR spectrum for **L3** ligand before photolysis recorded in D_2O at 298.1 K. The inset shows the labels used for the assignment of the signals

The ^1H NMR spectrum for the photolysed ligand (see Fig. 10) clearly reveals structural changes that involve a loss of symmetry of the molecule. In the aromatic region the signals for PY2 and PY4 are not equivalent, and the same occurs with the benzylic signal, which is now split in two different signals. It is also important to note the appearance of a singlet at 3.2 ppm not present in the spectrum of the sample before photolysis. To check the possibility that the signals could correspond to different compounds resulting from the breaking of **L3**, a DOSY experiment (Fig. 11) was carried out and it clearly indicated that the singlet at 3.2 ppm corresponds to a different compound with a lower molecular weight.

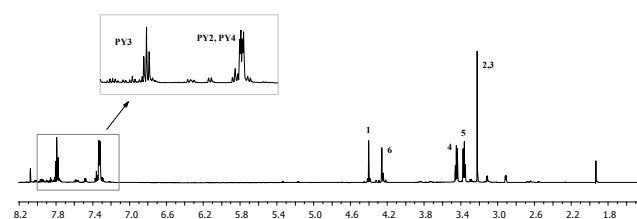


Fig. 10 ^1H NMR spectrum for **L3** ligand after photolysis recorded in D_2O at 298.1 K.

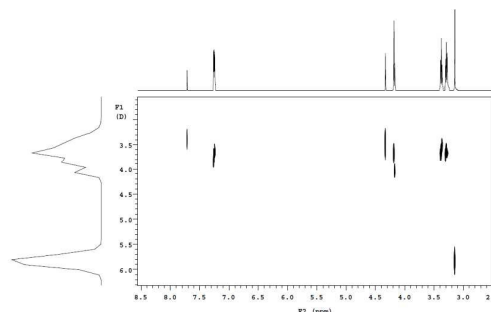


Fig. 11 DOSY spectrum for the photolysed ligand **L3** in D_2O at 298.1 K.

The ESI-MS spectrum of the photolysed sample shows a major signal at 181 m/z , which corresponds to a $[\text{L3}-\text{C}_2\text{H}_4+\text{H}]^+$ fragment resulting from decomposition of **L3**, whose $[\text{L3}+\text{H}]^+$ signal appears at 206. Thus, both the NMR and ESI-MS results support the occurrence of a photochemical process involving the breaking of **L3** to give a new **L3-C₂H₄** ligand and ethylene glycol (Fig. 12), a process not reported previously in this kind of ligands. However, this finding can be rationalized by considering that upon excitation in polar solvents as water, the dissociation of the C-N bonds in aliphatic amines becomes possible because the homolytic breaking of the N-H bond usually observed in less polar organic solvents is hindered by solvation.²⁴ In the present case, photochemical dissociation of a single C-N bond would lead to the breaking of the macrocycle with formation of NH_2 and CH_2OH fragments, so that the experimentally observed products would be the result of the same process occurring on the two C-N bonds of the same ethylenic chain.

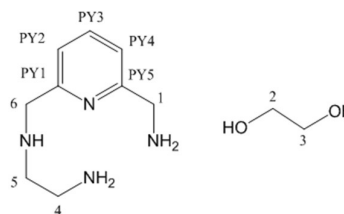


Fig. 12 The structure of products resulting from photolysis of **L3**

EXPERIMENTAL

The synthesis of the ligand **L1** has been carried out following the general procedure described in literature for the preparation of analogous receptors,¹⁰ which consists of reaction of the polyamine 6-(2'-aminoethyl)-3,6,9-triaza-1(2,6)-pyridinacyclodecaphane (**L2**) with fluorene-2-carboxaldehyde in ethanol followed by reduction with sodium borohydride, in order to obtain **L1**.

Synthesis of 5-[2-(N-2-fluorenyl)ethylamino]-2,5,8-triaza[9]-2,6-pyridinophane Trichlorohydrate (L1**·3HCl)** 6-(2'-aminoethyl)-3,6,9-triaza-1(2,6)-pyridinacyclodecaphane (0.69 g, 2.77 mmol) and fluorene-2-carboxaldehyde (0.54 g, 2.77 mmol) are dissolved in 100 mL of dry ethanol and stirred at

room temperature for 2 hours. Then sodium borohydride (1.1 g, 28 mmol) is added and the mixture is stirred for 2 more hours. Then, the solution is vacuum evaporated and extracted with CHCl_3 (6 x 50 mL). The organic phase is taken to dryness and re-dissolved in dry ethanol. The hydrochloride salt of the product is precipitated by adding a concentrated HCl solution. ^1H NMR (D_2O , 300 MHz): δ_{H} 2.92 (t, J = 5 Hz, 4H), 3.09 (t, J = 7 Hz, 2H), 3.26 (t, J = 5 Hz, 4H), 3.36 (t, J = 7 Hz, 2H), 4.02 (s, 2H), 4.38 (s, 2H), 4.64 (s, 4H), 7.46 (d, J = 8 Hz, 2H), 7.52 (t, J = 8 Hz, 3H), 7.69 (d, J = 7 Hz, 1H), 7.73 (s, 1H), 7.97 (t, J = 8 Hz, 2H). ^{13}C NMR (D_2O , 75.43 MHz): δ_{C} 36.7, 42.6, 46.2, 49.8, 50.8, 51.2, 52.1, 120.8, 120.9, 122.5, 125.8, 127.1, 127.5, 128.1, 129.1, 129.2, 140.1, 140.6, 142.9, 144.3, 144.9, 149.2. Anal Calcd. For $\text{C}_{27}\text{H}_{33}\text{N}_5\cdot 3\text{HCl}\cdot 2\text{H}_2\text{O}$: C, 59.0; H, 6.9; N, 11.5; Found: C, 56.6; H, 7.0; N, 12.2.

Synthesis of $[\text{PbL1}][\text{PbL1Cl}](\text{NO}_3)_2\cdot 4\text{H}_2\text{O}$ (1). To an aqueous solution (5 mL) of **L1**·3HCl (0.017 g, 0.038 mmol), $\text{Pb}(\text{NO}_3)_2$ (0.011 g, 0.03 mmol) in water (5 mL) was added dropwise with stirring. The pH of the solution was adjusted to 11 by addition of 0.5 M NaOH. After the mixture was stirred for 2 hours at room temperature, it was filtered. Crystals suitable for X-ray analysis were obtained by slow evaporation of the solvent.

Synthesis of $[\text{PbL3}](\text{ClO}_4)_2$ (2) To an aqueous solution (5 mL) of **L3**·3HBr (0.017 g, 0.038 mmol), $\text{Pb}(\text{NO}_3)_2$ (0.011 g, 0.03 mmol) in 0.15 M NaClO_4 (5 mL) was added dropwise with stirring. The pH of the solution was adjusted to 9 by addition of 0.5 M NaOH. After the mixture was stirred for 2 hours at room temperature, it was filtered. Crystals suitable for X-ray analysis were obtained by slow evaporation of the solvent.

Caution: Perchlorate salts of compounds containing organic ligands are potentially explosive and should be handled with care.

Crystallographic Analysis. Analysis on single crystals of **1** and **2** were carried out with an Oxford diffraction Supernova diffractometer at 120 K and Bruker-Nonius KAPPA CCD diffractometer ($\lambda = 0.71073 \text{ \AA}$) respectively. The structures were solved by direct methods using the program SHELXT²⁵ and refined by full-matrix least squares on all F^2 using SHELXL²⁵ with the OLEX2²⁶ suite. Molecular plots were produced with either the program MERCURY²⁷ Crystal data, data collection parameters, and results of analysis are listed in Table S1.

Structure **1** was solved in the orthorhombic space group Pbcn . Due its symmetry the two different cationic complexes are overlapping and they share in the same position the lead atom, the aromatic rings and the amine groups except amine N4. This amine and the ethylenic chains were placed in two different set of atoms modelled with an occupancy of 50% each one using PART instructions. The coordinated chloride (Cl1) anion, the nitrate anion, and the chloride counteranions and the water molecules placed in the voids between the complexes were also modelled with occupancy of 50%. The hydrogen atoms of the disordered water molecules could not be placed.

Some soft SHELXL restraints (DELU, ISOR, SIMU) had to be used to correct the geometry of the disordered parts and the thermal parameters of the corresponding atoms.

CCDC-1528996 and CCDC-1529381 contain the supplementary crystallographic data for this paper. These data can be obtained free of charge from The Cambridge Crystallographic Data Centre via www.ccdc.cam.ac.uk/data_request/cif.

EMF Measurements. The potentiometric titrations were carried out at $298.1 \pm 0.1 \text{ K}$ using NaNO_3 0.15 M or 0.15 M NaNO_3 , $\text{EtOH}:\text{H}_2\text{O}$ 30:70 as supporting electrolyte. The experimental procedure (burette, potentiometer, cell, stirrer, microcomputer, etc.) has been fully described elsewhere.²⁸

The acquisition of the emf data was performed with the computer program PASAT.²⁹ The reference electrode was a Ag/AgCl electrode in saturated KCl solution. The glass electrode was calibrated as a hydrogen-ion concentration probe by titration of previously standardized amounts of HCl with CO_2 -free NaOH solutions and the equivalent point determined by the Gran's method,³⁰ which gives the standard potential, E° , and the ionic product of water ($\text{pK}_w = 13.73(1)$).

The computer program HYPERQUAD was used to calculate the protonation and stability constants.³¹ The pH range investigated was 2.5–11.0 and the concentration of the metal ions and of the ligands ranged from 1×10^{-3} to $5 \times 10^{-3} \text{ M}$ with M:L molar ratios varying from 2:1 to 1:2. The different titration curves for each system (at least two) were treated either as a single set or as separated curves without significant variations in the values of the stability constants. Finally, the sets of data were merged together and treated simultaneously to give the final stability constants.

NMR Measurements. The ^1H and ^{13}C NMR spectra were recorded on a Bruker Avance AC-300 spectrometer operating at 299.95 MHz for ^1H and at 75.43 MHz for ^{13}C . The chemical shifts are given in parts per million referenced to the solvent signal. Adjustments to the desired pH were made using drops of DCl or NaOD solutions. The pD was calculated from the measured pH values using the correlation, $\text{pD} = \text{pH} - 0.4$.³²

The ^1H NMR spectra and the DOSY (Diffusion-Ordered Spectroscopy) experiment were recorded at 298.1 K using an Agilent Technologies spectrometer operating at 599.77 MHz. For the photolysis experiments, a sample was prepared using 11 mg of **L3** dissolved in D_2O (99% D) and then it was directly exposed to the light lamp of the stopped-flow for 20 hours in acidic conditions ($\text{pD} = 1.8$). The spectra of the photolysed **L3** products were obtained in conditions of solvent suppression to achieve a better signal to noise ratio.

Spectrophotometric and Spectrofluorimetric Titrations. Absorption spectra were recorded on a Shimadzu UV-2501 PC spectrophotometer. Fluorescence spectra were obtained with a PTI MO-5020 spectrofluorimeter. The emission spectra were measured from 300 to 500 nm for an excitation wavelength of 260 nm, corresponding to the maximum of the excitation intensity. HCl and NaOH were used to adjust the pH values that were measured with a Metrohm 713 pH meter in both cases.

Kinetic experiments The kinetic experiments were carried out at $298.1 \pm 0.1 \text{ K}$ using an Applied Photophysics SX17MV stopped-flow instrument provided with detectors for the simultaneous measurement of fluorescence and absorbance changes. A FSR-WG295 filter provided by Newport was placed

ARTICLE

Journal Name

in the fluorescence detector to cut-off any contribution from wavelengths below 295 nm. Preliminary experiments were carried out to determine the optimum wavelength for monitoring the fluorescence changes and then both the fluorescence and the absorbance changes at the excitation wavelength were simultaneously registered. The kinetic results obtained from absorbance measurements were checked with a Bio-Logic stopped-flow instrument provided with a diode array detector.

The kinetic studies on complex decomposition were carried out under pseudo-first-order conditions of acid excess and the solutions contained Pb^{2+} and the ligand in 1:1 molar ratio. The pH of the starting solutions of the metal complexes was selected from the species distribution curves so that the concentration for one of the complex species is maximum while maintaining low concentrations of the other ones. The ionic strength was adjusted to 0.15 M by adding the required amount of NaClO_4 or NaNO_3 , and the pH was adjusted by addition of the required amount of 0.15 M aqueous solutions of NaOH , HNO_3 or HClO_4 . No significant differences were observed when the anion was changed from $[\text{NO}_3^-]$ to $[\text{ClO}_4^-]$. Kinetic data were analyzed with the SPECFIT program.³³

Conclusions

The Pb^{2+} coordination chemistry of three related azamacrocyclic ligands (**L1-L3**) has been analyzed by potentiometry, NMR, UV-Vis and spectrofluorimetric titrations. The crystal structures $[\text{PbL1}][\text{PbL1Cl}](\text{NO}_3)\text{Cl}_2 \cdot 4\text{H}_2\text{O}$ (**1**) and $[\text{PbL3}](\text{ClO}_4)_2$ (**2**) revealed that the conformation of the macrocyclic core and the disposition of the metal ion is the same in both cases revealing the presence of a stereoactive lone pair. Moreover, although the secondary amino group of the pendant arm in **L1** is implicated in the coordination of the metal ion, the stereoactive effect of the lone pair prevents the complex to adopt the closed conformation which is typically found in other metal complexes of this kind of aza-scorpand like ligands.

Stopped-flow kinetic studies of the acid-promoted dissociation of the Pb^{2+} complexes of **L1-L3** using simultaneous absorbance and fluorescence detection indicate that, in spite of their similarity, the dissociation of the metal ion occurs with very different rates in the three complexes. During the course of the kinetic studies evidence was obtained for the occurrence of a photochemical process that leads to ligand degradation with the unexpected elimination of one CH_2CH_2 fragment from the macrocyclic core.

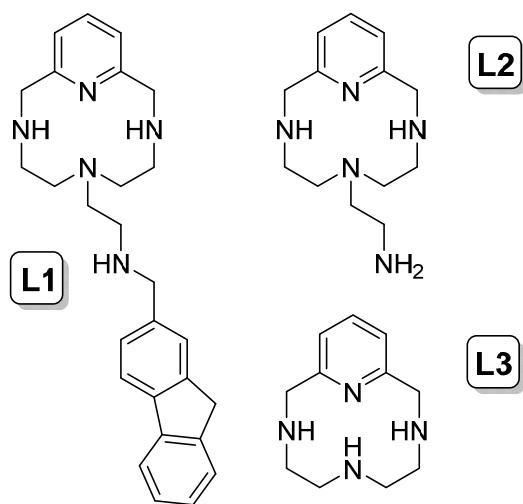
Acknowledgements

Financial support by the Spanish MICINN and MEC and FEDER funds from the European Union are gratefully acknowledged (grants CSD2010-00065, CTQ2015-65707-C2-2-P, CTQ2013-48917-C3-1-P and CTQ2016-78499-C6-1-R), Unidad de Excelencia María de Maeztu MDM-15-0538) and Generalitat Valenciana (PROMETEO II 2015-002).

Notes and references

- Agency for Toxic Substances and Disease Registry. Atlanta, Georgia, USA.
<http://www.atsdr.cdc.gov/csem/csem.asp?csem=7&po=10>
- (a) E. K. Jaffe, M. Volin and C. B. Mayers, *Biochemistry* 1994, **33**, 11554-11562; (b) E. K. Jaffe, *Comments Inorg. Chem.* 1993, **15**, 67-92; (c) L. W. Mitchell and E. K. Jaffe, *Arch. Biochem. Biophys.* 1993, **300**, 169-177; (d) E. K. Jaffe, W. R. Abrams, H. X. Kaempfen, and K. A. Harris Jr. *Biochemistry* 1992, **31**, 2113-2123; (e) E. K. Jaffe, G. D. Markham and J. S. Rajagopalan, *Biochemistry* 1990, **29**, 8345-8350; (f) A. J. Dent, D. Beyersmann, C. Block and S. S. Hasnain, *Biochemistry* 1990, **29**, 7822-7828; (g) E. K. Jaffe and D. Hanes, *J. Biol. Chem.* 1986, **261**, 9348-9353; (h) E. K. Jaffe and G. D. Markham, *Biochemistry* 1987, **26**, 4258-4264; (i) E. K. Jaffe and G. D. Markham, *Biochemistry* 1988, **27**, 4475-4481.
- J. Chisholm, *J. Sci. Am.* 1971, **224**, 15-23.
- J. M. Ratcliffe, *Lead in Man and Environment*; John Wiley & Sons: New York, 1981.
- (a) L. Shimoni-Livny, J. P. Glusker and C. W. Bock, *Inorg. Chem.* 1998, **37**, 1853-1867; (b) F. Ceccconi, C. A. Ghilardi, S. Midollini and A. Orlandini, *Inorg. Chim. Acta* 2000, **308**, 135-138.
- (a) D. L. Reger, M. F. Huff, A. L. Reingold and B. S. Haggerty, *J. Am. Chem. Soc.* 1992, **114**, 579-584; (b) J. S. Casas, García-M. S. Tasende and J. Sordo, *Coord. Chem. Rev.* 2000, **209**, 197-261.
- a) R. J. Andersen, R. C. diTargiani, R. D. Hancock, C. L. Stern, D. P. Goldberg and H. A. Godwin, *Inorg. Chem.* 2006, **45**, 6574-6576; (b) R. Pedrido, M. J. Romero, M. R. Bermejo, A. González-Noya, I. García-Lema and G. Zaragoza, *Chem. Eur. J.* 2008, **14**, 500-512; (c) R. Pedrido, M. R. Bermejo, M. J. Romero, M. Vázquez, A. M. González-Noya, M. Maneiro, M. J. Rodríguez and M. I. Fernández, *Dalton Trans.* 2005, 572-579; (d) G. Battistuzzi, M. Borsari, L. Menabue, M. Saladini and M. Sola, *Inorg. Chem.* 1996, **35**, 4239-4247.
- (a) C. Serena, E. Calvo, M. P. Clares, M. L. Diaz, J. U. Chicote, R. Beltrán-Debon, R. Fontova, A. Rodríguez, E. García-España and A. García-España, *Plos One* 2015, 1-12. <http://dx.doi.org/10.1371/journal.pone.0119102>; (b) M. P. Clares, C. Serena, S. Blasco, A. Nebot, L. del Castillo, C. Soriano, A. Domènech, A. V. Sánchez-Sánchez, L. Soler-Calero, J. L. Mullor, A. García-España and E. García-España, *J. Inorg. Biochem.* 2015, **143**, 1-8; (c) J. González-García, A. Martínez-Camarena, B. Verdejo, M. P. Clares, C. Soriano, E. García-España, H. R. Jiménez, A. Domènech-Carbó, R. Tejero, E. Calvo, L. Briansó-Llort, C. Serena, S. Trefler and A. García-España, *J. Inorg. Biochem.* 2016, **163**, 230-239; (d) E. García-España, M. P. Clares, S. Blasco, C. Soriano, J. González, B. Verdejo, *Patent* WO 2011/033163 A2.
- M. Inclán, M. T. Albelda, J. C. Frías, S. Blasco, B. Verdejo, C. Serena, C. Salat-Canela, M. L. Díaz, A. García-España and E. García-España, *J. Am. Chem. Soc.* 2012, **134**, 9644-9656.
- B. Verdejo, A. Ferrer, S. Blasco, C. E. Castillo, J. González, J. Latorre, M. A. Máñez, M. G. Basallote, C. Soriano and E. García-España, *Inorg. Chem.*, 2007, **46**, 5707-5719.
- K. Zhang, J. Geng, C. Jin and W. Huang, *Dalton Trans.*, 2014, **43**, 15351-15358.
- J. Costa and R. Delgado, *Inorg. Chem.* 1993, **32**, 5257-5265.
- S. Blasco, B. Verdejo, M. P. Clares, C. E. Castillo, A. G. Algarra, J. Latorre, M. A. Máñez, M. G. Basallote, C. Soriano and E. García-España, *Inorg. Chem.* 2010, **49**, 7016-7027.
- B. Verdejo, L. Acosta-Rueda, M. P. Clares, A. Aguinaco, M. G. Basallote, C. Soriano, R. Tejero and E. García-España *Inorg. Chem.*, 2015, **54**, 1983-1991.

- 15 (a) F. Cuenot, M. Meyer, E. Espinosa and R. Guillard, *Inorg. Chem.*, 2005, **44**, 7895-7910. (b) F. Cuenot, M. Meyer, E. Espinosa, A. Bucaille, R. Burgat, R. Guillard and C. Marichal-Westrich, *Eur. J. Inorg. Chem.* 2008, 267-283. (c) J. L. Laing, R. W. Taylor and C. A. Chang, *J. Chem. Soc. Dalton Trans.* 1997, 1195-1200. (d) V. C. Sekhar, C. A. Chang and S. Sherman, *Inorg. Chim. Acta*, 1987, **30**, 157-162.
- 16 A. Bencini, A. Bianchi, E. García-España, M. Micheloni and J. A. Ramírez, *Coord. Chem. Rev.* 1999, **188**, 97-156.
- 17 (a) M. Julliard and M. Chanon, *Chem. Rev.* 1983, **83**, 425-506; (b) A. P. de Silva and R. A. D. Dayasiri Rupasinghe, *J. Chem. Soc., Chem. Commun.* 1985, 1669-1670.
- 18 A. Bencini, M. A. Bernardo, A. Bianchi, E. García-España, C. Giorgi, S. Luis, F. Pina and B. Valtancoli, in G. W. Gokel (Ed). *Advances in Supramolecular Chemistry*, vol 8. Cerberus Press. Miami, 2002.
- 19 United States Environmental Protection Agency Roadmap for Mercury, EPA-HQ-OW-2015-0680, 2017.
- 20 R. D. Hancock, M. S. Shaikjee, S. M. Dobson and J. C. A. Boeyens, *Inorg. Chim. Acta* 1988, **154**, 229-238.
- 21 C. E. Castillo, M. A. Máñez, M. G. Basallote, M. P. Clares, S. Blasco and E. García-España, *Dalton Trans.*, 2012, **41**, 5617-5624
- 22 C. E. Castillo, J. González-García, J. M. Llinares, M. A. Máñez, H. R. Jiménez, E. García-España and M. G. Basallote, *Dalton Trans.*, 2013, **42**, 6131-6141.
- 23 L. H. Chen and C. S. Chung, *Inorg. Chem.*, 1989, **28**, 1402-1405.
- 24 Ya. N. Malkin and V. A. Kuz'min, *Russ. Chem. Rev.* 1985, **54**, 1041-1057.
- 25 G. M. Sheldrick, *Acta Crystallogr.*, 2015, **A71**, 3-8.
- 26 O. V. Dolomanov, L. J. Bourhis, R. J. Gildea, J. A. K. Howard and H. Puschmann, *J. Appl. Crystallogr.* 2009, **42**, 339-341.
- 27 P. R. Edgington, P. McCabe, C. F. Macrae, E. Pidcock, G. P. Shields, R. Taylor, M. Towler and J. v. d. Streek, *J. Appl. Crystallogr.* 2006, **39**, 453-457.
- 28 E. García-España, M.-J. Ballester, F. Lloret, J. M. Moratal, J. Faus and A. Bianchi, *J. Chem. Soc., Dalton Trans.* 1988, 101-104.
- 29 M. Fontanelli and M. Micheloni, Program for the automatic control of the microburette and the acquisition of the electromotive force readings (PASAT). *Proceedings of the I Spanish-Italian Congress of Thermodynamics of Metal Complexes*, Peñíscola, Castellón, Spain, 1990.
- 30 (a) G. Gran, *Analyst* 1952, **77**, 661-671; (b) F. J. Rossotti and H. Rossotti, *J. Chem. Educ.* 1965, **42**, 375-378.
- 31 P. Gans, A. Sabatini and A. Vacca, *Talanta* 1996, **43**, 1739-1753.
- 32 (a) P. K. Glasoe and F. A. Long, *J. Phys. Chem.*, 1960, **64**, 188-190; (b) A. K. Covington, M. Paabo, R. A. Robinson and R. G. Bates, *Anal. Chem.*, 1968, **40**, 700-706.
- 33 R. A. Binstead, B. Jung and A. D. Zuberbühler, SPECFIT-32, Spectrum Software Associates, Chappel Hill, 2000.



View Article Online
DOI: 10.1039/C7DT00680B

Chart 1

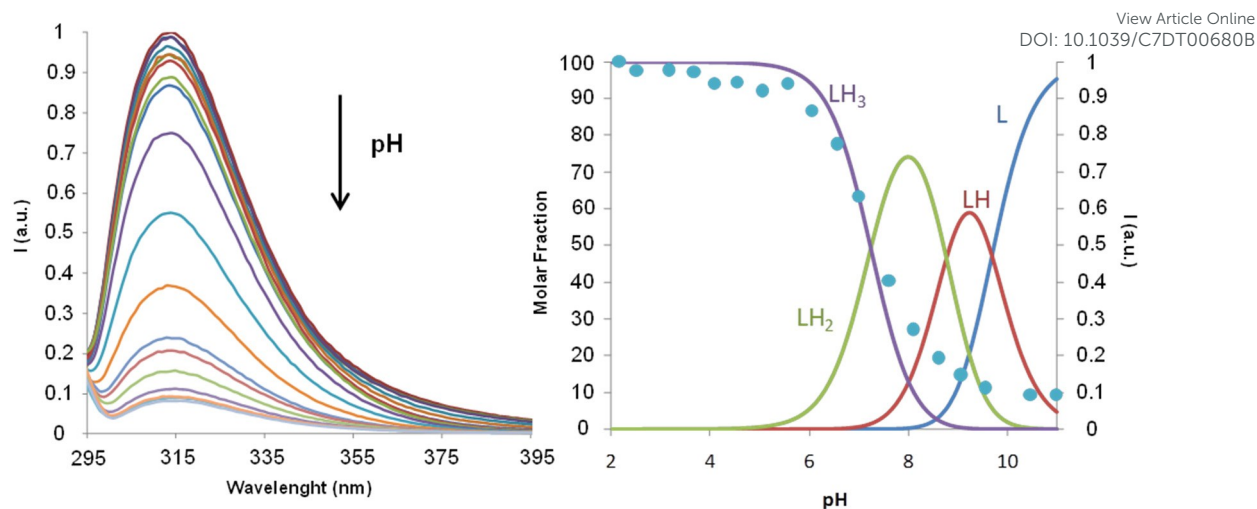


Fig. 1 (a) Fluorescence emission spectra of **L1** recorded at 298.1 K as function of pH. (b) Steady-state fluorescence emission titration curve of **L1** ($\lambda_{\text{exc}} = 285 \text{ nm}$) measured at $298.1 \pm 0.1 \text{ K}$ with $[\text{L1}] = 1.0 \times 10^{-5} \text{ M}$ (blue \bullet) and mole fraction distribution curves for the different protonated forms (solid lines).

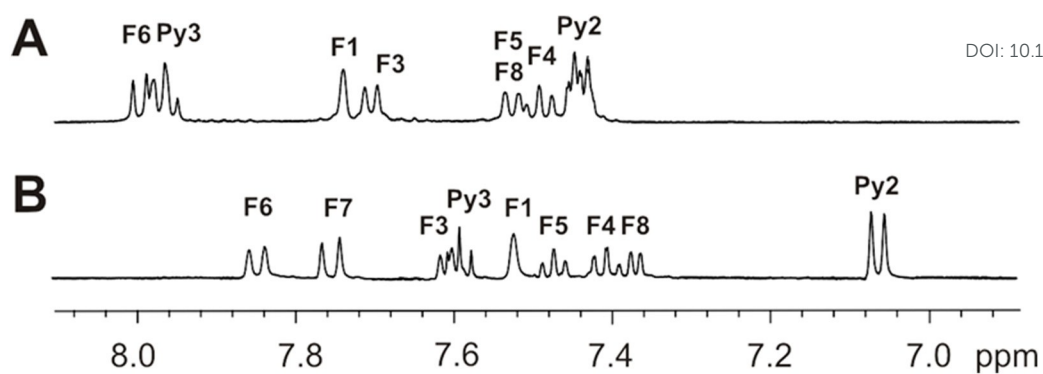


Fig. 2 ^1H NMR spectra of the aromatic region of **L1** recorded in D_2O at pD: (A) 3.23 and (B) 8.58.

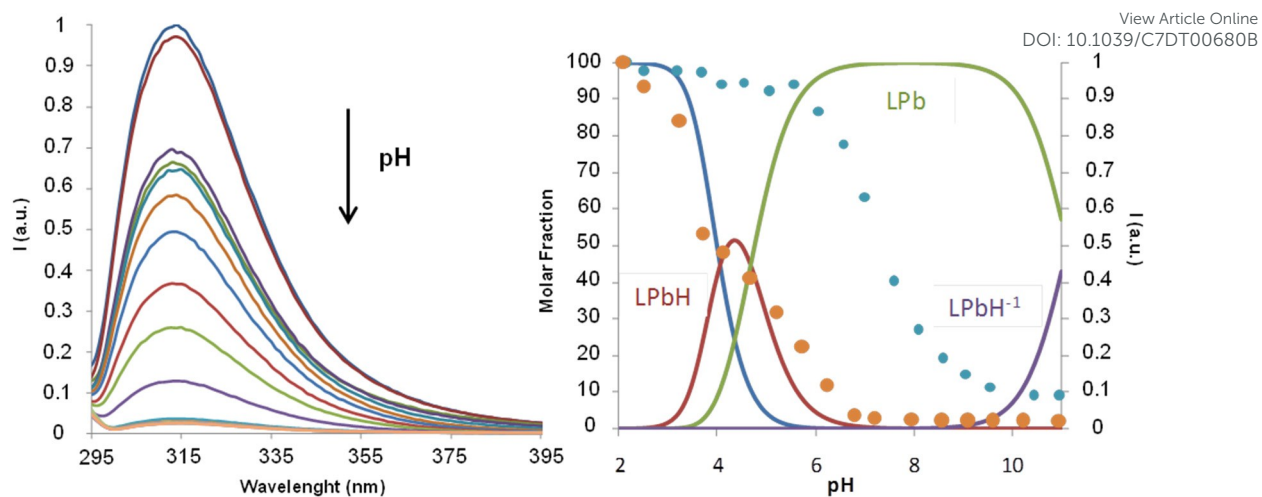


Fig. 3 (A) Fluorescence emission spectra of Pb^{2+} -**L1** recorded at 298.1 K as function of pH. (B) Steady-state fluorescence emission titration curves for the system Pb^{2+} -**L1** ($\lambda_{\text{exc}} = 285$ nm) in a 1:1 molar ratio M:L ($[\text{L1}] = [\text{Pb}^{2+}] = 10^{-5}$ M. Emission followed at 312 nm (free ligand ● blue, metal complexes ● orange) and mole fraction distribution curves for the Pb^{2+} complexes (solid lines).

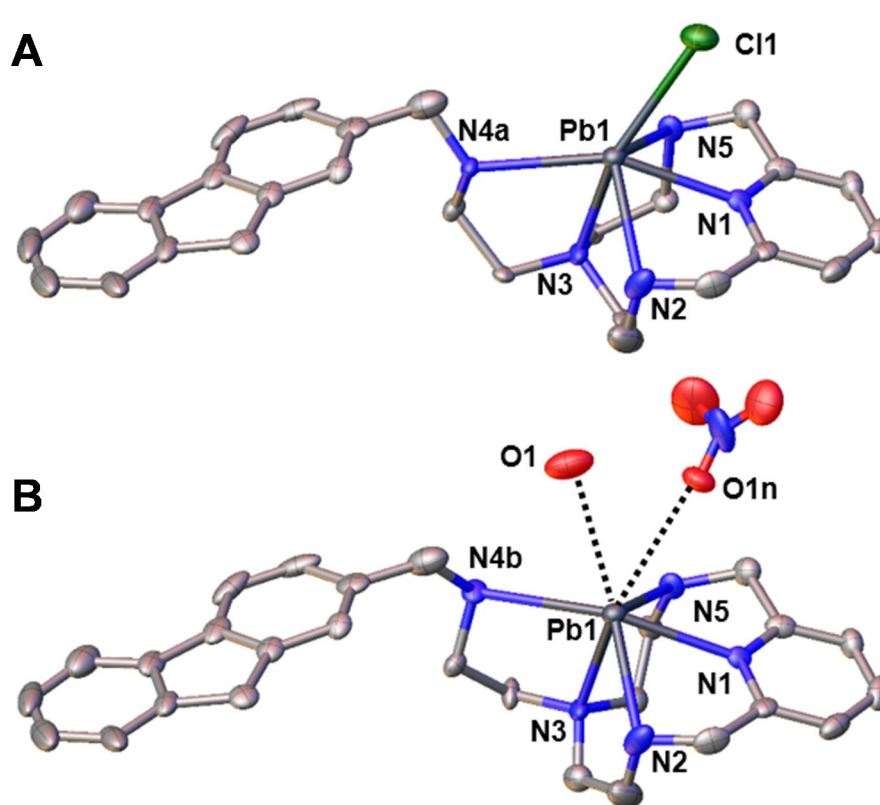


Fig. 4 Ellipsoid representation of the cationic species: a) $([\text{PbL1}](\text{NO}_3)(\text{H}_2\text{O}))^+$ and b) $[\text{PbL1Cl}]^+$. Thermal ellipsoids are shown at the 50% probability level. Hydrogen atoms have been omitted for clarity.

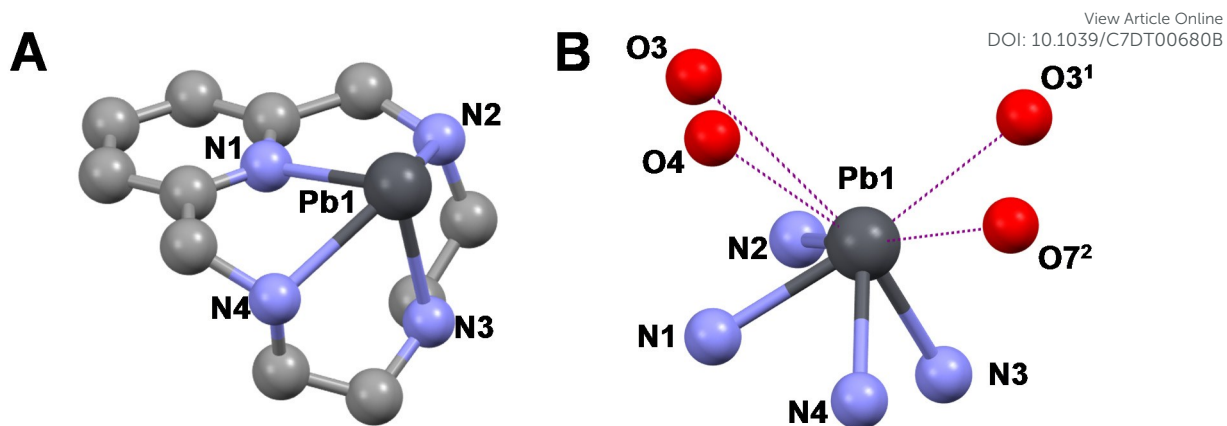


Fig. 5 (A) Ball and stick representation of the $[\text{PbL3}]^{2+}$ cation. Hydrogens are not shown. (B) Coordination site of Pb^{2+} in $[\text{PbL3}](\text{ClO}_4)_2$ showing the gap occupied by the lone pair.

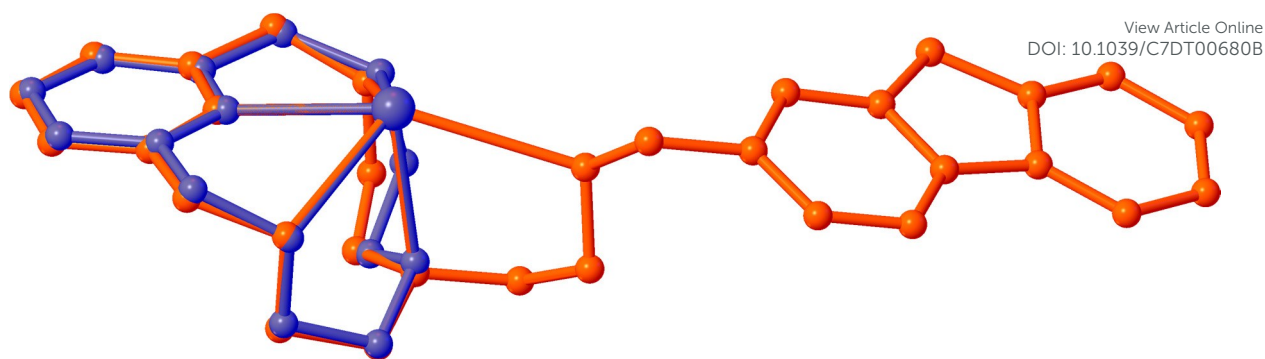


Fig. 6 Overlay representation of crystals $[\text{PbL1}]^{2+}$ (orange) and $[\text{PbL3}]^{2+}$ (blue) in order to highlight the similarities in the geometry of the ligand. Only the metal complexes are shown

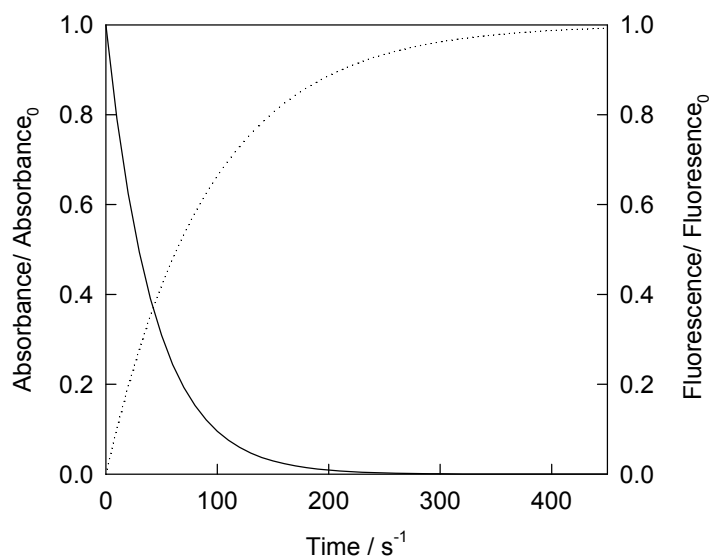


Fig. 7 Kinetic traces showing the absorbance (275 nm) (solid line) and fluorescence (excitation at 275 nm and detection at wavelengths larger than 295 nm) (dotted line) changes upon addition of an excess of acid (0.15 M) to a solution containing Pb^{2+} and **L3** ($[\text{Pb}]_0 = [\text{L3}]_0 = 5 \times 10^{-4}$ M) with the starting pH adjusted to 8.5. Both traces were recorded simultaneously on the same solution.

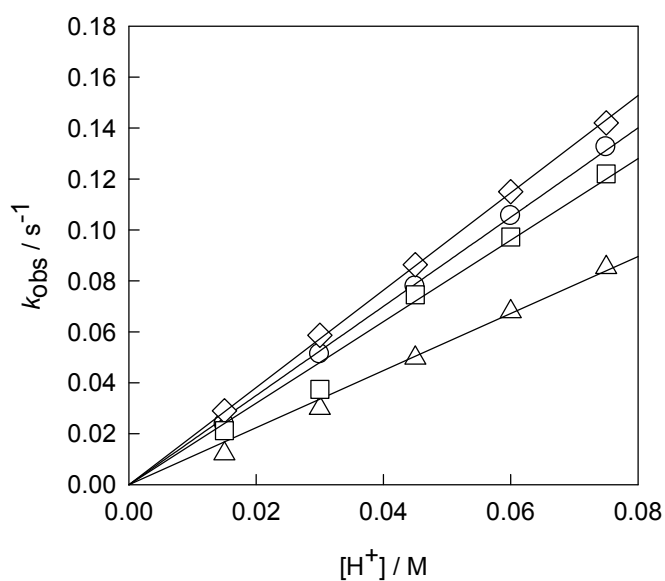


Fig. 8 Plots showing the dependence with the acid concentration of the observed rates constants for the decomposition of the Pb^{2+} -**L3** complexes: starting pH of 8.5 ($[\text{PbL3}]^{2+}$) with absorbance (circles) and fluorescence (triangles) detection, and starting pH of 3.3 (mixture of $[\text{Pb}(\text{HL3})]^{3+}$ and $[\text{PbL3}]^{2+}$) with absorbance (diamonds) and fluorescence (squares) detection.

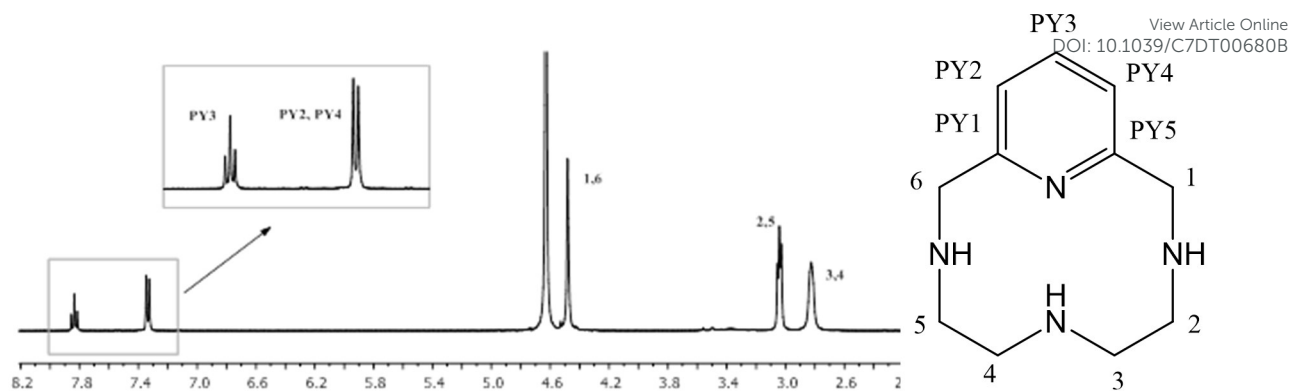


Fig. 9 ^1H NMR spectrum for L3 ligand before photolysis recorded in D_2O at 298.1 K. The inset shows the labels used for the assignment of the signals

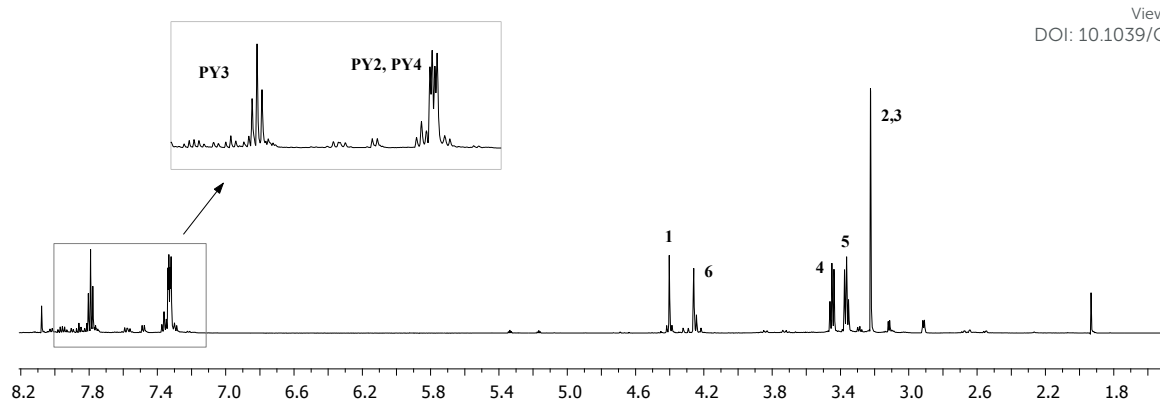


Fig. 10 ^1H NMR spectrum for L3 ligand after photolysis recorded in D_2O at 298.1 K.

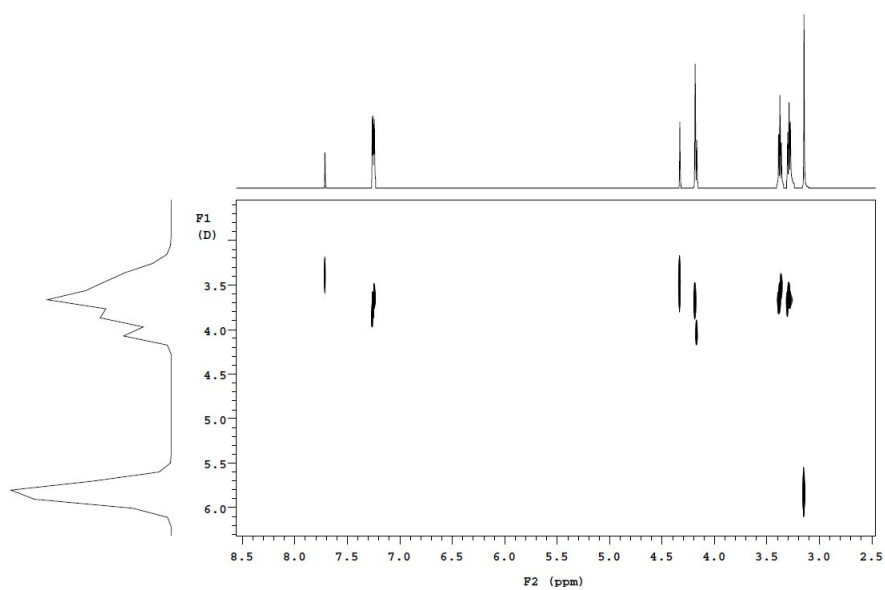
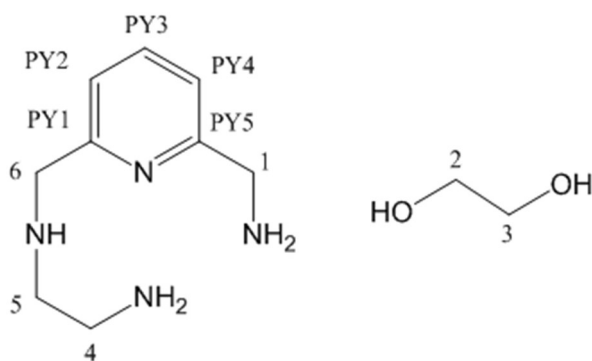


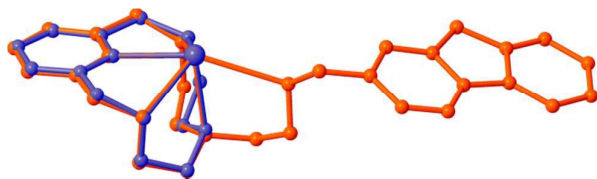
Fig. 11 DOSY spectrum for the photolysed ligand **L3** in D₂O at 298.1 K.



View Article Online
DOI: 10.1039/C7DT00680B

Fig. 12 The structure of products resulting from photolysis of **L3**

Table of Contents



The synthesis and Pb^{2+} coordination of azamacrocyclic ligands are described. The paper includes one of the few kinetic studies so far reported on the acid-promoted dissociation of Pb^{2+} macrocyclic complexes.